WATER RESEARCH 45 (2011) 5027–5037

Available at www.sciencedirect.com

ScienceDirect

journal homepage: www.elsevier.com/locate/watres

A simple optode based method for imaging O_2 distribution and dynamics in tap water biofilms

M. Staal [a,*], E.I. Prest [a,b], J.S. Vrouwenvelder [b,c], L.F. Rickelt [a], M. Kühl [a,d]

[a] Marine Biological Section, Department of Biology, University of Copenhagen, Strandpromenaden 5, DK-3000 Helsingør, Denmark
[b] Wetsus, Centre of Excellence for Sustainable Water Technology, P.O. Box 1113, 8900 CC Leeuwarden, The Netherlands
[c] Delft University of Technology, Department of Biotechnology, Julianalaan 67, 2628 BC Delft, The Netherlands
[d] Plant Functional Biology and Climate Change Cluster (C3), Department of Environmental Science, University of Technology Sydney, Broadway NSW 2007, Australia

ARTICLE INFO

Article history:
Received 2 February 2011
Received in revised form
25 May 2011
Accepted 3 July 2011
Available online 13 July 2011

Keywords:
Oxygen sensing
Planar optodes
Lifetime
Imaging
Membrane fouling simulator
Biofilm

ABSTRACT

A ratiometric luminescence intensity imaging approach is presented, which enables spatial O_2 measurements in biofilm reactors with transparent planar O_2 optodes. Optodes consist of an O_2 sensitive luminescent dye immobilized in a 1–10 μm thick polymeric layer on a transparent carrier, e.g. a glass window. The method is based on sequential imaging of the O_2 dependent luminescence intensity, which are subsequently normalized with luminescent intensity images recorded under anoxic conditions. We present 2-dimensional O_2 distribution images at the base of a tap water biofilm measured with the new ratiometric method and compare the results with O_2 distribution images obtained in the same biofilm reactor with luminescence lifetime imaging. Using conventional digital cameras, such simple normalized luminescence intensity imaging can yield images of 2-dimensional O_2 distributions with a high signal-to-noise ratio and spatial resolution comparable or even surpassing those obtained with expensive and complex luminescence lifetime imaging systems. The method can be applied to biofilm growth incubators allowing intermittent experimental shifts to anoxic conditions or in systems, in which the O_2 concentration is depleted during incubation.

1. Introduction

Biofilms are surface-associated microbial communities exhibiting spatio-temporal heterogeneity in their structure, composition, physiology and chemical microenvironment (Costerton et al., 1995; Stewart and Franklin, 2008). Such communities represent the preferred lifestyle of many microbes in natural ecosystems, and biofilms also play important roles in more applied contexts such as waste water treatment and industrial processes (Nicolella et al., 2000), chronic infections (Costerton et al., 1999; Hall-Stoodley et al., 2004), and e.g. corrosion and biofouling of materials (Ridgway and Flemming, 1996; Vrouwenvelder et al., 2008).

The growth dynamics and complex structural heterogeneity of biofilms has been studied in great detail, especially through application of various microscopic techniques (Neu et al., 2010). However, a similar detailed mapping of the chemical landscape and dynamics in biofilms is lacking in

Abbreviations: ROI, region of interest; MFS, membrane fouling simulator; mil, 1 mil equals 25.4 μm; Ru-dpp, Ruthenium(II)-tris-4,7-diphenyl-1,10-phenanthroline; PS, polystyrene.

* *Corresponding author*. Tel.: +45 3532098; fax: +45 35321951.
E-mail address: Mstaal@bio.ku.dk (M. Staal).

0043-1354/$ – see front matter © 2011 Elsevier Ltd. All rights reserved.
doi:10.1016/j.watres.2011.07.007

most studies. Electrochemical and fiber-optic microsensors (Revsbech, 2005; Kühl, 2005) can provide very detailed information on local chemical dynamics, zonations of microbial processes and mass transfer processes in biofilms (e.g. de Beer et al., 1994; Stoodley et al., 1994; Kühl and Jørgensen, 1992; Kühl et al., 1996), but such 1-dimensional characterization is in most cases inadequate to assess the true spatial distribution and dynamics of the chemical microenvironment in heterogeneous biofilms at similar resolution as biofilm structure can be resolved (Jørgensen and Des Marais, 1990). Modeling of biofilm systems has shown that significant differences can be found between 1- and 2-dimensional descriptions of biofilms, since 1-dimensional models fail to describe spatial heterogeneity other than over depth (z-plane). It has also been argued from biofilm modeling approaches that it is sufficient to do 2-dimensional measurements for a proper description of spatial heterogeneity in microenvironments, since increasing model complexity from 2- to 3-dimensions did not yield much extra insights (Eberl et al., 2000). However, there is still a lack of real datasets linking spatial biofilm heterogeneity to chemical heterogeneities and microenvironments.

With the development of imaging techniques, several new non-invasive methods became available, e.g. Confocal Laser Scanning Microscopy (Neu et al., 2010), Raman Microspectroscopy (Ivleva et al., 2010), lifetime imaging (Glud et al., 1996; Hidalgo et al., 2009), Magnetic Resonance Microscopy (Wagner et al., 2010). These methods allow measurements of 2- and 3-dimensional chemical and biological landscapes in biofilms. Molecular oxygen (O_2) is a key parameter in biogeochemical and biological studies (Glud, 2008; Fenchel and Finlay, 2008) and the introduction of planar optodes for mapping 2-dimensional O_2 concentration in natural systems (Glud et al., 1996) was a big step forward for the study of the heterogeneity of O_2 distribution and dynamics in sediments and biofilms (e.g. Glud et al., 1998, 1999; Kühl et al., 2007). Such planar optode measurements are based on luminescent indicator dyes, immobilized in a polymeric matrix and cast onto a transparent carrier. The measuring principle relies on the dynamic quenching of indicator luminescence by O_2. Both the luminescence intensity (I) and luminescence lifetime (τ) vary reversibly with O_2 concentration, and the process does not consume O_2. The ideal response of such optical O_2 sensors is described by the Stern–Volmer relation (Bacon and Demas, 1987):

$$\frac{I}{I_0} = \frac{\tau}{\tau_0} = \frac{1}{1 + K_{SV}[O_2]} \Leftrightarrow \frac{I_0}{I} = \frac{\tau_0}{\tau} = 1 + K_{SV}[O_2] \quad (1)$$

where τ_0 and τ denote the luminescence lifetime in the absence and in the presence of O_2 respectively; I_0 and I denote the luminescence intensity in the absence or presence of O_2; K_{SV} is the bimolecular quenching coefficient of the dye in its specific polymeric matrix, and $[O_2]$ is the O_2 concentration. In practice, most planar optodes exhibit a non-ideal Stern–Volmer like response, which can be modeled with a two-component model (Carraway et al., 1991), where only a certain fraction of the O_2 indicator dye remains quenchable upon immobilization. This relationship can be described by the equation:

$$\frac{I}{I_0} = \frac{\tau}{\tau_0} = \frac{1 - \alpha}{1 + K_{sv}C} + \alpha \quad (2)$$

where α is the non-quenchable fraction. Initial applications of O_2 planar optodes involved simple luminescence intensity measurements in combination with planar optodes with a black O_2 permeable overcoat to avoid optical artifacts from background light and sample backscatter (Glud et al., 1996). Application of transparent O_2 optodes on glass allows direct alignment of O_2 distribution to the structure of the sample (e.g. Holst and Grunwald, 2001; Kühl et al., 2007, 2008, Staal et al., 2011) and nowadays oxygen imaging with planar optods makes almost entirely use of luminescent lifetime imaging systems (Holst et al., 1998; Oguri et al., 2006). Such systems are mostly custom built and relatively expensive (>30.000 €), which has been a bottleneck for the more widespread distribution of planar O_2 optode methodology. Recently, however, a new ratiometric method has been published using a normal digital single-lens reflex camera as detector (Wang et al., 2010; Larsen et al., in press). In this method, correction for an uneven light field was accomplished by inclusion of a luminescent O_2 insensitive reference dye in the planar optode matrix. Both dyes are excited by the same excitation source, but the reference dye emits light in the green region, and the O_2 sensitive dye in the red region, coinciding with the green and red channels of common color camera CCD or CMOS detectors. A ratio of the red and green channel indicates the O_2 concentration.

Here we present a simple luminescence intensity imaging approach enabling 2-dimensional mapping of biomass and O_2 concentration in a biofilm growth incubator using simple digital color cameras or monochromatic cameras combined with suitable emission filters. The method uses the ratio of the luminescence from a transparent planar optode under anoxia to the luminescence under experimental O_2 conditions to correct for heterogeneity in excitation light. No reference dye is required. As a proof of principle, a heterotrophic biofilm was grown on top of a transparent planar optode, which created heterogeneity in O_2 concentrations. We show that such a simple imaging approach yields information on the 2-dimensional distribution of O_2 in biofilms with a good signal-to-noise ratio and with a spatial resolution of 36 μm/pixel comparable or better than in more elaborate lifetime based O_2 imaging.

2. Methods

The planar O_2 optode used in this study was based on the luminescent O_2 sensitive dye Ruthenium(II)-tris-4,7-diphenyl-1,10-phenanthroline (Ru-dpp) immobilized in a polystyrene (PS) matrix (20 mg Ru-dpp/g PS). Such Ru-dpp based planar optodes are suitable for O_2 imaging over a wide dynamic range (up to full O_2 saturation) (Kühl and Polerecky, 2008). The PS/Ru-dpp mixture was dissolved in chloroform (3.3 w/w%) and cast onto a silanized glass plate (Kühl et al., 2007). After slow evaporation of the solvent in a semi-closed container, this resulted in a ~9 μm thick homogeneous O_2 sensor layer on the complete glass window of the incubator (6 cm × 28 cm).

The coated glass plate was mounted as a window in a watertight flow-trough biofilm growth incubator, i.e., a membrane fouling simulator (MFS), where a polypropylene spacer mesh was placed on top of the optode surface. The

biofilm growth chamber had external dimensions of 0.07 m × 0.30 m × 0.04m (Vrouwenvelder et al., 2006, 2007). Coupons of feed spacer, membrane and product spacer were placed in the MFS resulting in the same spatial dimensions and orientation as in spiral wound membrane elements applied in water treatment. For MFS experiments, membranes and 787 μm (31 mil) thick feed spacer sheets were taken from a new, unused spiral wound reverse osmosis membrane element. The development of fouling, i.e. biofilm formation, was monitored by a rhodamine tracer dye imaging technique (see below) and by measuring the pressure drop increase over the feed spacer channel of the MFS. During operation, the MFS window was covered with a light-tight lid to prevent growth of phototrophic organisms.

The reactor system setup consisted of a pressure reducing valve, manometer, dosage point (for biodegradable compounds), MFS and flow controller (Fig. 1, Vrouwenvelder et al., 2007). An extra T-connection was placed in the tubing before the inlet of the biofilm monitor to allow injection of saturated sodium dithionite solution to create anoxic conditions, as well as injection of water colored by the dye rhodamine WT (Chrompton & Knowles OT/US 04029NS). The dye Rhodamine WT is an inert, non-adsorbing and stable tracer for flow visualization and is simple to quantify by light absorbance (Huettel et al., 1996). The MFS was sterilized for a period of 5 min with 70% ethanol before the start of the experiment. Bacteria in the biofilm originated from bacteria occurring in the drinking water system. The MFS was operated at 16 °C. A pressure of 120 kPa was applied to avoid degassing. The feed water flow was 16 L h^{-1} equal to a linear flow velocity of 0.16 m s^{-1}, representative for the linear flow velocity in the lead membrane element in full-scale installations containing spiral wound nanofiltration or reverse osmosis membrane elements (Vrouwenvelder et al., 2009a). The MFSs were operated single pass without (partial) recirculation. Pressure drop measurements were performed with a pressure difference transducer (Deltabar S: PMD70-AAA7FKYAAA, Endress & Hauser, The Netherlands). The calibrated measuring range was 0–50 kPa (Vrouwenvelder et al., 2009b).

Concentrated substrate was dosed into the feed water (tap water), prior to the MFS by a peristaltic pump (Masterflex L/S brushless digital drive, HV 7523.70, 1.6–100 rpm, with an Easy Load II pump rotor, Applicon Analytical, The Netherlands) at a flow of 0.03 L h^{-1} from a 5L stock solution reservoir. The dosage of substrate was checked periodically by measuring the water volume pumped over a defined time interval. The chemicals $NaCH_3COO$, $NaNO_3$ and NaH_2PO_4 were dosed in a mass ratio C:N:P of 100:20:10 with a concentration of 1.0 mg acetate-C L^{-1} in the feed water entering the MFS. The substrates were dissolved in MilliQ water. To restrict bacterial growth in the substrate dosage bottle, the pH was set at 11 by NaOH dosage. Stock solution bottles were replaced every 5 days. The substrate flow rate (0.03 L h^{-1}) was low compared to the feed water flow rate (16 L h^{-1}). Thus, the effect of the substrate flow on the pH of the feed water was insignificant.

2.1. *Imaging systems and image calculations*

Two different camera systems were used for O_2 measurements: (1) A monochrome 12 bit fast gate-able cooled 1280X1024 CCD chip camera (2/3" chip), denoted as the PCO camerain this manuscript (SENSICAM-SENSIMOD, PCO AG, Kehlheim, Germany) and controlled by custom made acquisition software (Look@MOLLI, Holst and Grunwald, 2001) that can perform intensity based as well as lifetime based O_2 imaging (Holst et al., 1998); (2) A 8 bit color 1280X1024 CMOS chip camera (1/2" chip), denoted as the μEye camerain this manuscript (USB μEye SE,UI-1540-C, IDS Imaging Development Systems GMBH, Obersulm, Germany) and controlled by the manufacturers acquisition software. The μEye camera can only perform intensity based O_2 imaging. Both image acquisition programs allowed manual programming of the exposure time of the camera chips. The gain per color channel could be set manually in the software for the μEye camera allowing separate signal optimization of the three color channels.

For measurements with the μEye camera, the camera was coupled via a C-mount to a 2X magnification objective with an additional focusing lens (Microbench basic set, Qioptiq, Germany); the same optical setup was also mounted on the PCO camera for direct comparisons. The focal distance was

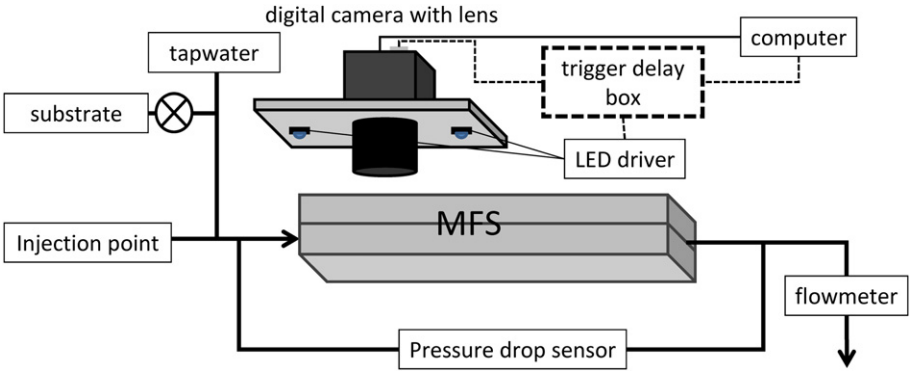

Fig. 1 – Schematic description of the membrane fouling simulator (MFS) including a water mixing system, pressure-drop sensor, flow meter and the imaging setup for O_2 detection. The camera was a cooled PCO monochrome cooled CCD camera or a μEye color CMOS camera. The trigger-delay box and the control of the LED driver (both indicated with dashed lines) are only present in the lifetime setup with the fast gate-able digital camera (PCO camera). The black arrows indicate the flow direction. There is no flow via the pressure-drop sensor.

~1.5 cm. A long pass filter (>590 nm) was placed in between the camera chip and the lens to exclude background and reflected blue excitation light. With a binning of 2, the resolution of this setup is ~36 μm per pixel. Additional measurements with the PCO camera were done with a Xenoplan XNP 1.4/17 objective (Schneider-Kreutznach, Germany) equipped with a long pass filter (>590 nm, Schneider-Kreutznach, Germany) and distance macro rings (2 mm) on the PCO camera to shorten the minimum focal distance from 15 to 5–10 cm. The resolution with this setup is ~72 μm per pixel. Background light was further diminished by a black card box mounted around the camera setup.

For the O_2 measurements with the PCO camera, two modulated power LEDs were used for excitation of the optode (1W Luxeon Star, 470 nm, Lumileds, San Jose; USA), as controlled by a custom built trigger-delay box. The two LEDs were mounted next to the lens. For lifetime imaging, the PCO camera was used in a modulated measuring mode, in which luminescence intensity images were acquired sequentially by integrating series of 3 μs imaging periods starting respectively at 0.1 (I_{W1}) μs and 4.1 (I_{W2}) μs after the 4 μs long excitation pulses, and followed by dark image acquisition (see also fig. X-1 and table X-1, additional information). The total integration time per measurement period was 500 ms (see Holst et al., 1998 for a detailed description of the measuring method and program). Lifetime (τ) images were subsequently calculated from the luminescence intensity images I_{W1} and I_{W2} images according to

$$\tau = \frac{\Delta t}{\ln\left(I_{W1}/I_{W2}\right)} \tag{3}$$

where Δt is the time difference between I_{W1} and I_{W2}.

For the ratiometric imaging method, we calculated the O_2 concentration from the ratio of luminescence images (I_0/I) taken under complete anoxic conditions (I_0) and oxygenated conditions (I), respectively (see also fig. X-1 and table X-1, additional information). In measurements with the PCO camera system, we also used the I_{W1} images to calculate O_2 images based on the ratio I_{0W1}/I_{W1}, thus allowing direct comparison of image quality by both lifetime and intensity based imaging. Additionally, intensity based measurements were also done using the intensity image setting in Look@MOlli, where the O_2 dependent luminescence intensity is measured during the blue LED excitation period, in contrast to the I_{w1} images taken 0.1 μs after the excitation flash. The integration time for the intensity images was shorter (100 μs) than for the lifetime measurements (to measure comparable intensities as in the lifetime images), while the excitation pulse length was equal (4 μs). The measuring time per pulse was 3 μs. Dark images were automatically taken and subtracted in the image acquisition program.

For the μEye color camera measurements, two power LEDs (1W Luxeon Star, 470 nm, Lumileds, San Jose; USA) were used for excitation of the optode. The LED light intensities were controlled by a stable and adjustable DC voltage source (GPC-3030DQ, GW Instek, Tucheng City, Taiwan) allowing precise control of current and voltage. The exposure time for the μEye camera was 200 ms (see also table X-1, additional information) and the gain for the blue, green and red channel were set to 80, 85 and 12, respectively, to optimize the gray value distribution over the three color channels.

Calibration of the optode in the MFS was done by circulating water with different O_2 concentrations at a stabilized temperature. The O_2 concentration in the water was changed by flushing the water with a series of set gas mixtures, mixed by a PC controlled automated gas mixing system based on electronic mass flow controllers (SensorSense, Nijmegen, Netherlands).

2.2. *Rhodamine assay*

Imaging of biofilm thickness in the MFS was performed to compare O_2 distribution with biomass distribution. Imaging was performed with the μEye camera without the long pass filter and samples were illuminated with 2 warm white LED strips (Hide-a-lite, Electro Elco AB, Sweden). A volume of 20 ml of a dilute rhodamine WT solution was injected into the MFS to measure the biofilm thickness. Rhodamine WT absorbs green-orange light, and absorption was measured by the green channel of the camera. If the measurement was carried out immediately after injection of the solution, rhodamine was only present in the flow channels, i.e. places were no biofilm was present. Calibration of the relationship between absorption and thickness was done with a triangle shaped glass cuvette with a thickness range of 0–700 μm, filled with the rhodamine solution (appendix, Fig X-2 and X-3,). A membrane (equal to the one in the MFS) was placed behind the cuvette to have the same light reflection characteristics as in the MFS. Images of the calibration cuvette were made at the same camera distance and illumination geometry as used for the biofilm thickness measurements in the MFS.

All image calculations (O_2 sensing and rhodamine assay) were done in the freeware ImageJ (version 1.45a; http://rsb.info.nih.gov/ij). After import to ImageJ, the color RGB images were split. All images were converted to a 32 bit floating point format before initial thresholding. Thresholding was performed to exclude low intensity pixels, i.e. pixels within areas where no fluorescence was measured (for example areas with marker ink), from further calculations (i.e ratio calculations, lifetime calculations etc). Ratio images were calculated using the "process→ image calculator" option in ImageJ. The color camera images were split into their Red, Green and Blue channels prior to ratio calculations, by using the "image→color→split channels" option in ImageJ. False coloring of the images was applied to visualize/emphasize differences in O_2 concentration. All data handling in ImageJ was done manually.

3. Results

3.1. *Calibration*

For calibration, lifetime images and luminescent intensity images of a clean optode (without biofilm) were recorded at 5 different O_2 concentrations. From these images, we calculated ratio images for the ratios τ_0/τ, I_{0W1}/I_{W1} of the PCO camera and the I_0/I of the red channel of the μEye camera at the different O_2 concentrations (Fig. 2), and we averaged the values of

a region of interest (1.6×10^5 pixels), comprising half of the imaged area. Selection of the regions of interest was done to exclude areas in the image without oxygen sensitive dye as well as areas with pixel values below a threshold grey value (<30). All three imaging methods showed a linear relationship with O_2 concentration ($r^2 > 0.99$), indicating that the non-quenchable fraction (α) was small. While the calibration curves of the different methods showed some variations, the use of different linear correlations to convert I_0/I into oxygen concentrations (see caption in Fig. 2) allowed us to compare the calculated O_2 images based on measurements with the different methods.

3.2. *Comparison of different methods*

To evaluate the performance of the ratiometric and the lifetime approach, we compared O_2 images based on luminescence images taken with the PCO camera (2X lens mounted) using different calculation and measuring methods (Fig. 3). All pictures were taken from exactly the same area of the planar optode in the biofilm growth incubator (MFS). The biofilm in the MFS had been growing for a period of 10 days. The luminescence images under full anoxic conditions (I_0 and I_{0w1}) were taken after injection of saturated sodium dithionite solution into the MFS. Images (I and I_{w1}) and lifetime images (I_{w1} and I_{w2}) in the presence of O_2 were taken, while oxygenated medium was flowing through the MFS.

The O_2 distribution on the optode surface was highly heterogeneous due to variations in biofilm thickness. The biofilm partially blocked the water flow causing formation of flow channels in the exopolymer matrix. All three O_2 images showed the same spatial O_2 distribution patterns, and the O_2 concentrations were in the same range. However, the O_2 images based on the ratio method I_{0W1}/I_{W1} or I_0/I (Fig. 3) showed much more details, as compared to the lifetime images.

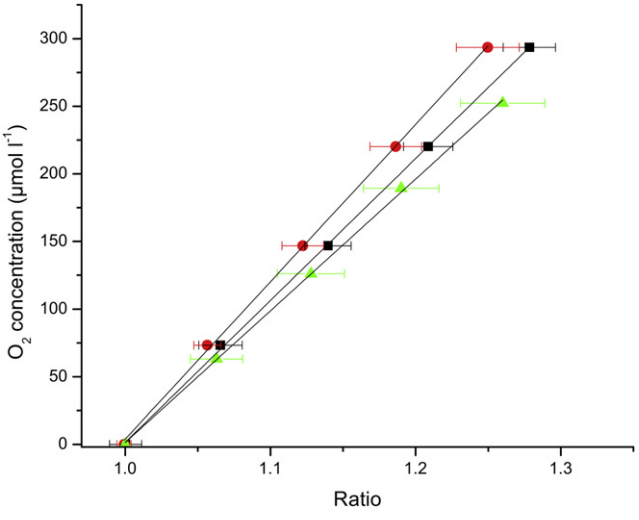

Fig. 2 – Calibration curves of the O_2 dependent ratios of τ_0/τ ($y = 1049.8x - 1048.5$, circles, $K_{sv} = 9.53 \times 10^{-4}$), the intensity I_{0W1}/I_{W1} ($y = 1164.5x - 1160.2$, squares, $K_{sv} = 8.59 \times 10^{-4}$) both measured with the PCO camera, and the I_0/I ratio of the luminescence intensity in the red channel measured with the µEye camera ($y = 974.8x - 973.6$, triangles, $K_{sv} = 1.03 \times 10^{-3}$). The linear correlation (r^2) for all curves was >0.999. The points represent average values of 1.6×10^5 pixels in a square Regions Of Interest (ROI) in the center of the image. Error bars denote the standard deviations of the ratio values of the pixels.

The biofilm in the MFS formed up to 0.8 mm thick structures due to the support of the spacer mesh (Fig. 4). Formation of such thick biofilms caused an increased pressure gradient within the MFS (data not shown) forcing medium through narrow channels. The flow channels were visualized by injection of rhodamine WT solution into the MFS (Fig. 4C).

The µEye and many other color cameras allow manual gain setting of the separate color channels to optimize the pixel saturation per channel. For O_2 sensing, we used the intensity histograms of each color channel in the camera program at anoxia (highest luminescence) to optimize the gain settings of every channel. In this way, no pixels were oversaturated in any of the channels, while ensuring optimal signal-to-noise ratio. With such optimized gain settings, it was possible to see differences in fluorescence intensity, even without splitting the three channels (Fig. 5A). However, proper calculation of O_2 images from the color camera .tiff format images still required splitting of the three channels.

We used the red channel for O_2 calculation since the emission spectrum of the Ru-dpp indicator (max. emission 610 nm) coincided best with the spectral range of the red channel. There was also a visible change in the green channel upon changing O_2 concentration, while the blue channel did not show much variation. There was no biofilm growth in the MFS during the calibration, and the O_2 concentration was considered homogeneous within the field of view. However, there was a clear intensity difference visible (Fig. 5B), due to spatial variation in excitation light and lens effects (Fig. 5C). After calculation of the ratio image, such heterogeneity was gone (Fig. 5D, E) and the image ratio showed a homogeneous response of the planar optode area in the camera field of view to the different O_2 concentrations.

To compare the ratio images from the µEye setup with the lifetime images of the PCO setup, we analyzed a position in the MFS that was imaged by both camera systems, consecutively (Fig. 6). Both lifetime and ratio images measured with the µEye camera yielded relatively noisy images, as compared to the ratio I_{0W1}/I_{W1} image and the I_0/I image made with the PCO camera (Fig. 3B, D). However, a structured O_2 distribution due to flow channel formation within the biofilm was still clearly visible. Closer inspection of the images showed that the O_2 distribution did not match exactly in the two image types. This difference is most likely caused by repetitive changes in flow rate. In our setup, we had to stop the flow to inject the saturated dithionite solution for the anoxic measurement before the flow was started again. This can result in detachment of part of the biofilm structure. In our example, most of the structure stayed intact and the images are still comparable (Fig. 6).

3.3. *Heterogeneity of O_2 distribution and consumption*

The highest O_2 concentrations were generally found in areas with no or little biofilm formation (Fig. 4D), while low O_2 zones developed away from the flow channels in areas with thick

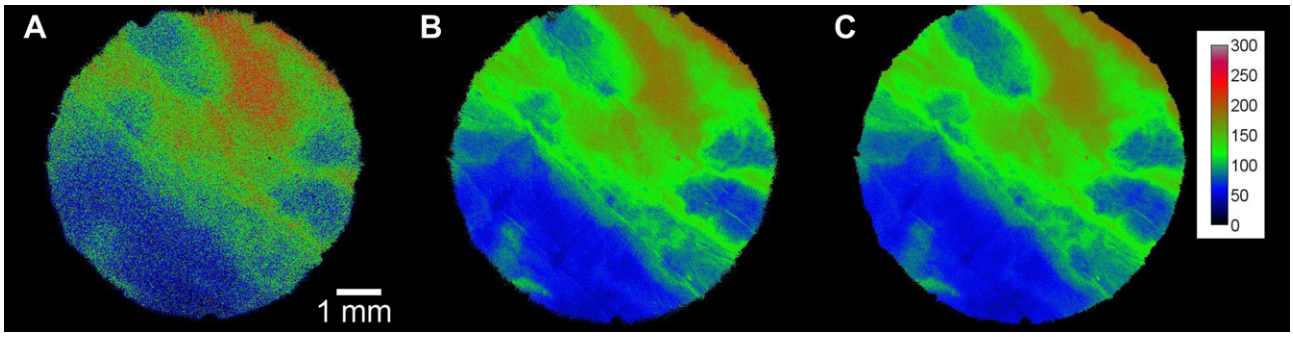

Fig. 3 – Images of O_2 distribution in the biofilm growth incubator (MFS) as measured with a 12 bit PCO camera system with a 2X magnification microscope lens mounted. The O_2 concentrations in the images are calculated from lifetime imaging (A), the ratio of the I_{W1} images (I_{0W1}/I_{W1}) under anoxic conditions (I_{0W1}) and under oxygenated conditions (I_{W1}) (B), and the ratio of the luminescence intensity (I_0/I) of images recorded under anoxic and oxygenated conditions, respectively (C). The color bar indicates the O_2 concentration in μmol l^{-1}. (For interpretation of the references to colour in this figure legend, the reader is referred to the web version of this article.)

biofilm and little water movement. However, overlaying the O_2 image with the biofilm distribution image also showed some zones with relative dense biofilm formation and relative high O_2 concentrations, as well as some regions exhibiting low O_2 concentrations without thick biofilm formation. The low O_2 zones did not reach complete anoxia at the optode surface (Fig. 4A, B). No differences were found between the two imaging approaches. The average O_2 concentration was 25 ± 13 μmol l^{-1} in the largest O_2 depleted zone (Fig. 7A left side, Region Of Interest (ROI) 1), while the O_2 concentration in other depleted zones was 52 ± 13 μmol l^{-1}. The O_2 concentration reached zero within these regions ~60–90 s after the flow in the biofilm monitor was stopped. In comparison, the O_2 concentration in the biofilm flow channels was 152 ± 23 μmol l^{-1} and became anoxic 100–150 s after the flow was stopped.

We estimated the O_2 depletion rate by measuring a series of O_2 images after stopping the flow with a frequency of 1 image per 10 s, and by subsequent subtraction of images in such time series. Lifetime images were generally too noisy to acquire accurate O_2 depletion rate images based on two sequential images, and averaging of 4–5 sequential images was necessary. However, the ratio (I_{0w1}/I_{w1}) based O_2 images were less noisy, and with these images it was possible to calculate O_2 depletion rates images without averaging.

The initial O_2 depletion rate (Fig. 7) in the channels measured by the ratio method was ~3.57 ± 1.97 μmol l^{-1} s^{-1} (average value of 6.3 × 10^4 pixels), which was 2–4 times the depletion rate (1.30 ± 1.39 μmol l^{-1} s^{-1} average value of 2.9 × 10^4 pixels) found in the low O_2 zones (ROI1 excluded). However, this was partly caused by the difference in initial O_2 concentration at the moment the flow was stopped (Fig. 7B). Oxygen depletion rates in the different channel regions were about 30% higher (1.85 ± 1.98 μmol l^{-1} s^{-1}) at ~50 μmol l^{-1} (average 50 ± 24 μmol l^{-1}). The large zone with low O_2 on the left site (ROI1) had a lower O_2 depletion rate 0.65 ± 1.31 μmol l^{-1} s^{-1} at 25 ± 14 μmol l^{-1} (3X10^4 pixels, while the other low O_2 zones had a depletion rate of 1.00 ± 1.28 μmol l^{-1} s^{-1} at an average O_2 concentration of 29 ± 12 μmol l^{-1}. The O_2 depletion rates in the channels were 1.15 ± 1.38 μmol l^{-1} s^{-1} at an average O_2 concentration of 31 ± 19 μmol l^{-1}. The O_2 depletion rates seemed equal for all 10 ROI's at O_2 concentrations below ~20 μmol l^{-1} (Fig. 7B). The respiration rates found in this study are within the ranges found using micro-electrodes (0.3–5 μmol l^{-1} s^{-1}) (Nielsen et al., 1990; Satoh et al., 2005).

4. Discussion

4.1. *Comparison of the different imaging techniques*

All three imaging methods showed a linear relationship between O_2 concentration and τ_0/τ, I_{0w1}/I_{w1} and I_0/I, indicating a low non-quenchable fraction of the indicator in the planar optodes used in this study. In principle, this linear relationship for the range 0–300 μmol l^{-1} O_2 allows a simple two point calibration.

The calibration images made with the color camera (Fig. 5) showed that the ratio approach corrects for variation in the luminescence intensity due to heterogeneity in the light field and lens effects. This makes the method applicable for imaging in systems even when the light distribution of the excitation lights is not perfectly homogeneous. A prerequisite is, however, that the measured area can be made anoxic without physical change or movement of the setup. In our case, we created anoxic conditions of the monitored area by addition of dithionite via an injection port in the tubing or by stopping the flow of the medium. But even though we took care not to touch the camera or MFS, the image position sometimes changed in between capturing images, due to minute movement of the MFS relative to the camera. The shift was only 2 or 3 pixels, but is enough to create erroneous results. The risk of movement is much bigger in our system than in the lifetime setting, since nothing is physically touched in between the recording of the lifetime images. The time difference between the recording is much smaller than for the I_0/I images. However, within ImageJ it can be easily checked whether the images are still aligned and, if necessary, the images can be repositioned based on chosen reference points within both images.

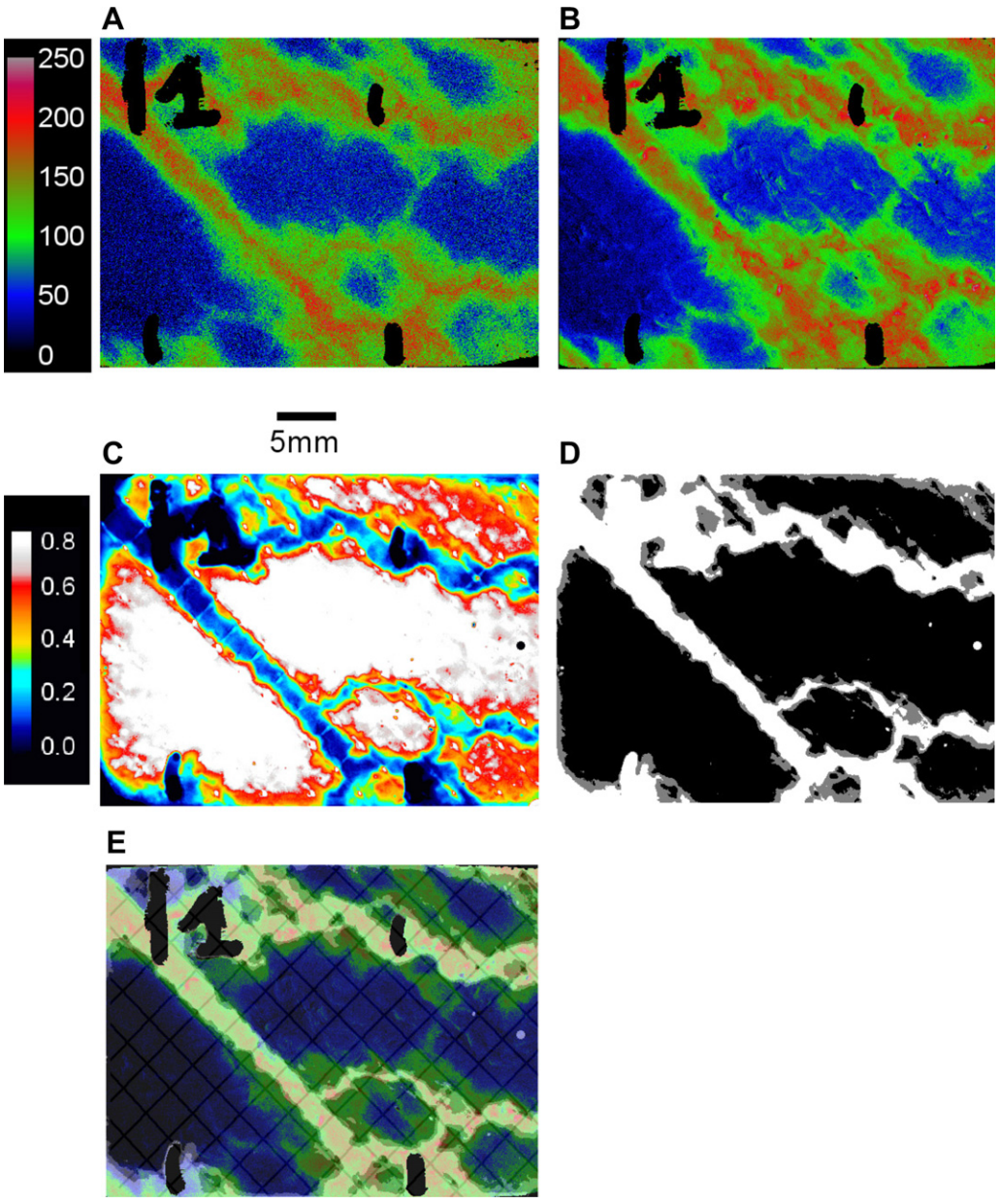

Fig. 4 – Images of O_2 concentration in an MFS harboring mature biofilms (10 days old). The O_2 was measured using luminescence lifetime imaging (A), and by taking the ratio between luminescence intensity images measured under anoxia and under experimental conditions (B). The heterogeneity in O_2 concentration is mostly caused by channel formation within the incubator. The color bar indicates the O_2 concentration in $\mu mol\ l^{-1}$. (C) Visualization of the water channels in the same position. The color bar indicates the water volume of moving water based on light absorption in the green channel after injection of rhodamine WT solution into the MFS. The color bar of C indicates the biofilm thickness in mm. After tresholding the image in panel C a mask is created with two different ranges of biofilm thicknesses. The white areas of the mask (D) indicate the open channel, the gray shaded zones indicate areas where the biofilm was 0.1–0.3 mm thick, while black zones indicate >0.3 mm thick biofilms. Panel E shows the O_2 image (B) combined with the a mask (D) made of the biofilm distribution image. Panel F shows the oxygen image with the support mesh overlayed. (For interpretation of the references to colour in this figure legend, the reader is referred to the web version of this article.)

The ratio I_0/I images from the color camera did not have the same spatial accuracy as the ratio based oxygen images from the PCO camera. This is not surprising, given that the PCO camera had a more sensitive cooled CCD chip with a bit depth of 12, while the color camera had a simple CMOS chip with a depth of 8 bit. A bit depth of 12 results in a 16 times larger dynamic range as compared to 8 bit cameras, and thus a much higher accuracy in the calculation of the ratio. However, the resolution, even with our relatively simple 8 bit color camera was almost as good as the resolution of the lifetime images. The accuracy may easily be improved by using better cameras e.g. with a bit depth of 12 per color channel. Cameras with a bit

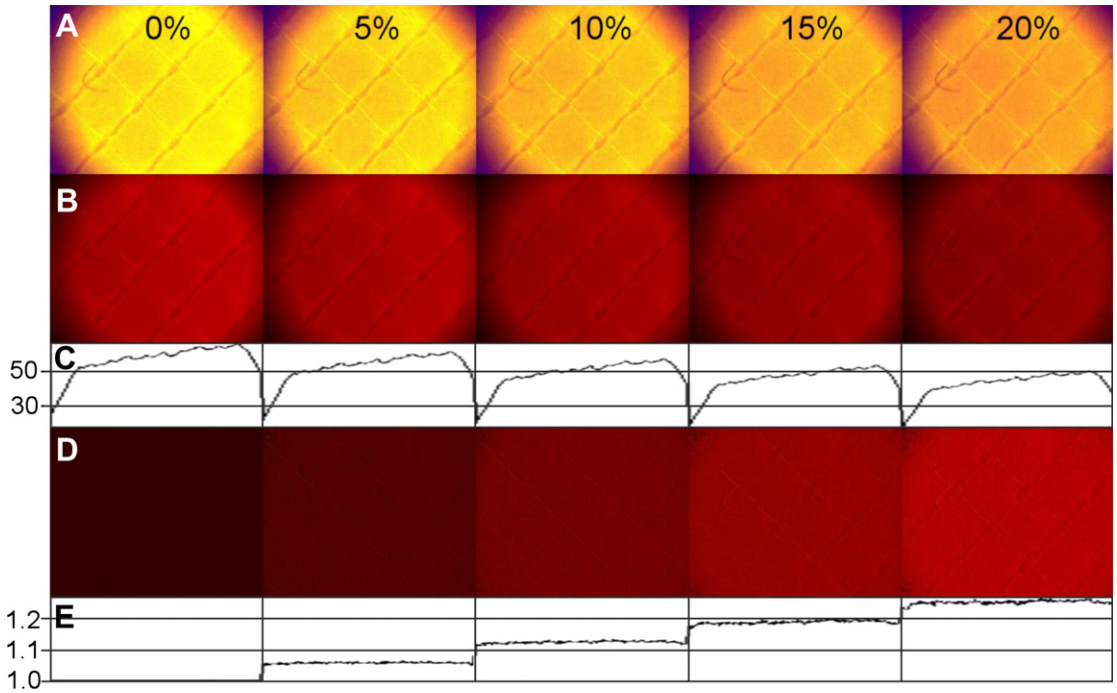

Fig. 5 – Luminescence intensity images at different O_2 levels (expressed as % O_2 in gas phase) (A) from an O_2 sensitive planar optode mounted in an MFS measured with the μEye camera (8 bit color). (B) the red channel of the color images, (C) the average gray values of the red channel, (D) images of the ratioI_0/I. (D) the average value of the ratio (E). (For interpretation of the references to colour in this figure legend, the reader is referred to the web version of this article.)

depth of 12 and cooled down to −30 °C below ambient temperature can be found nowadays for prices starting under 1000 € (e.g. cameras from Tucsen inc., China or Optic Star, United Kingdom), which is substantially below costs and efforts involved in establishing a luminescent lifetime system.

The O_2 images calculated from lifetime measurements had a lower resolution than the images based on the ratio I_0/I. The higher resolution of the I_0/I ratio approach thus allowed visualization of O_2 gradients, which were not clearly visible in the lifetime images. The reason for the difference in spatial resolution may be caused by the exponential character of lifetime images. Taking the exponent of the ratio I_{w1}/I_{w2}, as is done in the lifetime images, increases the noise level of the oxygen image. There was no obvious difference in resolution between the I_{0w1}/I_{w1} and I_0/I.

Another imaging approach based on intensity images, rather than on lifetime was used in the very first planar optode applications (Glud et al., 1996, 1999), where K_{sv} and α in Equation (2) were determined by measuring luminescence intensity images at 0%, 20%, and 100% O_2. Subsequently, the

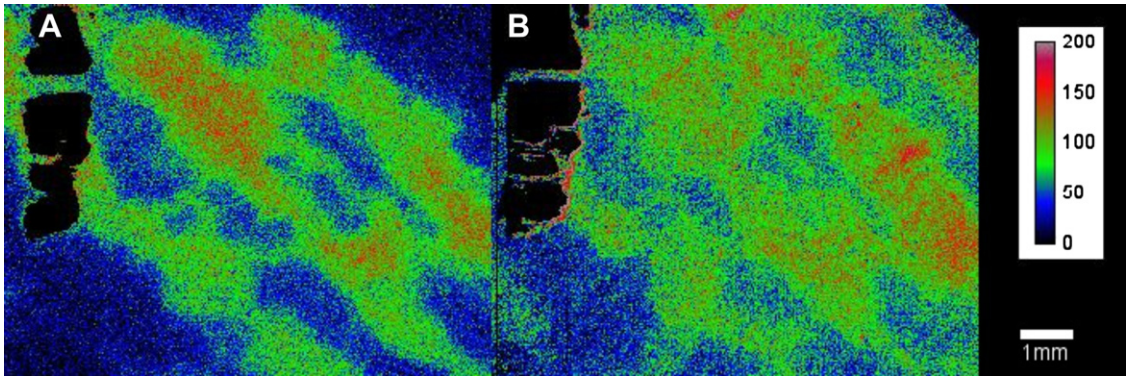

Fig. 6 – Comparison of lifetime image obtained with the PCO camera (A), and a I_0/I image (B) as calculated from the red channel images of the 8 bit μEye color camera from approximately the same area in the MFS. The I_0/I was reduced in size to correct for differences in pixel size. Positioning and resizing was based on the black ink structure (upper left) drawn on the glass window. The color bar indicates the O_2 concentration in μmol l^{-1}. The black areas are caused by marks made with a black permanent marker on the window. (For interpretation of the references to colour in this figure legend, the reader is referred to the web version of this article.)

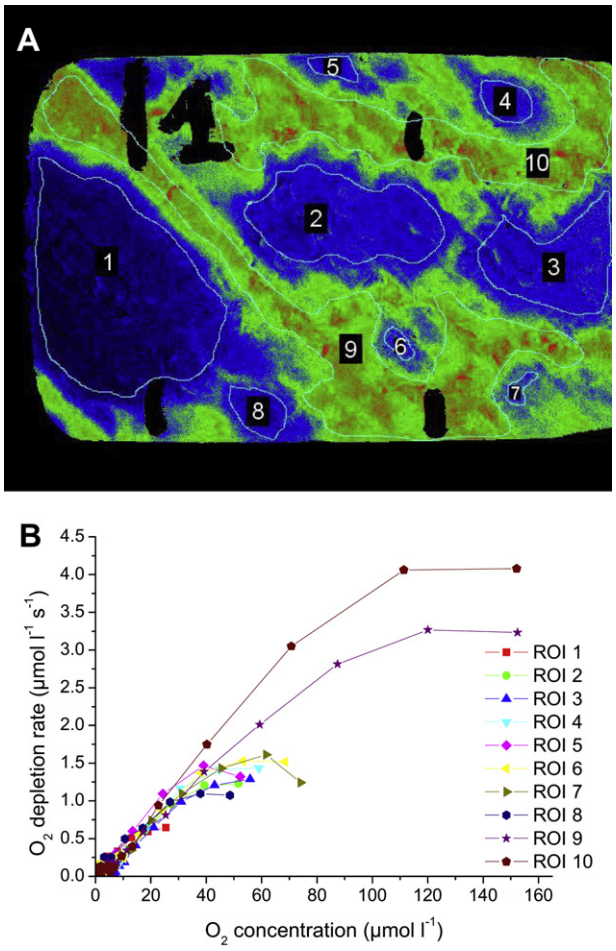

Fig. 7 – Relationship between O_2 concentration and O_2 depletion rate for 10 regions of interest (ROIs) in the MFS. Panel A shows an O_2 distribution image with a selection of different ROIs from which the depletion rates were measured. Panel Bshows the relationship in the areas where water is flowing freely (ROI 9 and 10), as well as in the low O_2 zones, characterized by the absence of free moving water (ROI 1-8). The points in the graphs indicate the average O_2 depletion rates at average O_2 concentration values of the ROI's indicated in the legend.

K_{sv} and α images where used to convert experimental luminescence intensity images to O_2 concentration images. While yielding high quality O_2 images, this approach required the use of non-transparent planar optodes as pure intensity based O_2 imaging is prone to light field variations and e.g. scattering artifacts from the sample structure (Holst et al., 1998). This method also requires the camera not be moved relative to the optode.

In the setup presented here, the O_2-dependent image ratio is calculated directly from the ratio of an image obtained under anoxic conditions and an image under a given O_2 concentration. The conversion from ratio to O_2 image is carried out by a linear correlation. This correlation can be determined prior to or afterward actual experiments and is not done at pixel level. Therefore it is not required that the optode has exactly the same position relative to the camera during calibration, yielding a relatively flexible and robust, yet simple O_2 imaging setup.

In our case, the image ratio had a linear relationship to O_2 concentration over 0–300 µmol l^{-1}, but also non-linear relationships can be used for the conversion within ImageJ. It has been found that other types of fluorescent dyes have non-linear relationships with O_2 concentration e.g. due to a substantial non-quenchable fraction of the immobilized indicator (Carraway et al., 1991). For planar optodes exhibiting a linear relationship between image ratios and O_2 concentration, it is possible to calculate dynamic changes (e.g. during experimental light–dark shift or stop-flow) without making an image under anoxic conditions simply by calculating the ratio of two consecutive luminescence intensity images multiplied by the slope found in the O_2 calibration curve.

4.1.1. *O_2 heterogeneity in the biofilm monitor*

The O_2 distribution was heterogeneous in the MFS after biofilm development. There was a good agreement with the distribution of free moving water and the higher O_2 concentrations. It seems logic that O_2 concentrations are higher in channels since little biomass is present in the channels, while water is flowing relatively fast. Advective transport is important in these regions, and fast flowing water will result in thin boundary layers, while little biomass is present. The O_2 concentration at the optode surface depends on the thickness of the diffusive boundary layer on top of the biofilm, the thickness of the biofilm on top of the optode and the O_2 consumption rate within the biofilm. However, some regions seemed to deviate from the relationship between water volume and higher O_2 concentration. This may partly be explained by the fact that the rhodamine method to estimate the free moving water did not discriminate for the distance at which the water flows from the optode. When half of the space is filled with biofilm, the free moving water may flow directly over the optode, but it may also be that the biofilm is between the optode and the water. Both situations will give the same absorbance, but will result in different O_2 concentrations at the optode surface. This illustrates the current limitations in our ability to experimentally resolve spatially complex chemical landscapes and mass transfer phenomena in biofilms.

It was surprising that O_2 was not fully depleted in regions without flowing medium. These regions did only become anoxic after stopping the flow in the MFS, while the lowest O_2 concentration under flow conditions in the MFS was ~25 µmol l^{-1}. Advective flow through the biofilm as reported in several studies (Costerton et al., 1999; Stewart and Franklin, 2008) could explain the observation. Since these channels are extremely small (a few µm) advective flow will be relatively slow due to a high resistance. This flow may have been overlooked by the rhodamine method used in this study. We only injected 20 ml rhodamine solution, prior to stopping the flow. This was enough to penetrate the main channels, but may not enough to show a flow in areas almost completely filled with biofilm.

Another explanation may be that the diffusion of the organic substrate into the biofilm is slow, and not in balance with the diffusion of O_2. This would result in the consumption of all organic material in the zones next to the channels, while

not all O_2 is consumed. The stop-flow experiments showed that the O_2 depletion rate was indeed relatively low in the biofilm zones (Fig. 4, left side). The O_2 depletion rate was almost 2 times lower compared to the depletion rate in the channel regions, while the biomass was assumed to be much higher in the biofilm zones. This could indicate that the biofilm in the low O_2 zones is either inactive or limited by organic substrates rather than by O_2. However, there was still some consumption in these regions, as shown by the onset of anoxic conditions when flow was stopped. Actually, biofilm regions reached anoxia before the channel regions turned anoxic.

4.1.2. *O_2 depletion and the stop-flow technique*

The O_2 concentrations in the medium at the inlet and outlet of the MFS were measured daily with an O_2 fiber optode showing that the O_2 concentration in the medium dropped by 25 μmol l^{-1} during its residence in the MFS, while O_2 imaging experiments were conducted. At the moment of the planar optode measurement, the flow was reduced from 16 to 2.7 L h^{-1} due to resistance caused by the biofilm formation. This would result in a total O_2 consumption rate of 18.7 nmol s^{-1} in the MFS. The average O_2 depletion rate measured using the stop-flow technique was 2.2 μmol l^{-1} s^{-1} for the monitored region. The free volume of the MFS was 6.5 ml, resulting in a total O_2 consumption rate of the whole monitor of 14.3 nmol s^{-1}. This value is rather close to the value estimated by measuring the O_2 decrease between the inlet and the outlet, although it is a bit lower. One explanation for the lower value may be that the O_2 sensor used to measure O_2 concentrations in the inlet and outlet measures in the tubing a bit out of the monitor. Since biofilms will also form in the tubing, this will add an extra consumption component to the system, resulting in a higher consumption rate. The stop-flow technique combined with the planar optode does not involve the tubing. Another explanation is that the surface area that was monitored does not reflect the behavior of the total incubator perfectly. In general, these two methods yield the same overall results, but the imaging method gives much more information on the heterogeneity in process rates.

Many microelectrode studies are published, showing oxygen gradients and oxygen fluxes in biofilms, but volumetric O_2 respiration rates of biofilms were determined in only few publications. Several volumetric respiration rates found with microelectrode studies were within the same range as the O_2 depletion rates found in this study (0.3–5 μmol l^{-1} s^{-1}, e.g. see Nielsen et al., 1990; Satoh et al., 2005). Therefore we feel that the O_2 depletion rates found with the ratiometric imaging approach are representative for the respiration rates of the biofilm. More extreme values, ranging from 0.03 (Polerecky et al., 2005) to 50 μmol l^{-1} s^{-1} (De Beer and Costerton, 2006) have also been reported, but the differences found may rather result from environmental factors like temperature, availability of organic substrate, etc. than from the method used. With the planar optode it can be assumed that the oxygen depletion rate reflects the oxygen consumption rate of the thin layer just on top of the optode, especially when the oxygen decrease is measured during the first 10 s after the flow is stopped. Stopping the flow will disrupt the steady state O_2 gradient and therefore reflect the respiration rate (Staal et al., 2011). After 5–10 s the O_2 depletion rate will become increasingly affected by a change in flux from overlaying layers.

5. Conclusions

It can be concluded that the I_0/I ratio approach for O_2 imaging with transparent planar O_2 optodes can be considered a good and more simple alternative to more elaborate luminescence lifetime imaging approaches. However, our approach can only be used in systems were the O_2 concentration can be reduced to zero without physical movement of the MFS relative to the camera. Such mechanical stability can easily be achieved in most biofilm reactor setups. A very simple imaging setup for imaging O_2 in biofilm reactors can be established from inexpensive commercial CCD or CMOS cameras and high intensity LEDs. The image analysis can be performed by powerful freeware such as ImageJ. In line with other recent ratiometric O_2 imaging approaches (Wang et al., 2010; Larsen et al., in press), this simplifies O_2 imaging and makes it more accessible for the research community. Here we presented O_2 distribution images measured at the base of a biofilm, but with some modifications in the experimental setup it is also possible to measure the O_2 distribution inside granules or biofilms.

Appendix. Supplementary material

Supplementary data associated with this article can be found, in the online version, at doi:10.1016/j.watres.2011.07.007.

REFERENCES

Bacon, J., Demas, J., 1987. Determination of oxygen concentrations by luminescence quenching of a polymer-immobilized transition-metal complex. Analytical Chemistry 59, 2780–2785.

Carraway, E.R., Demas, J.N., DeGraff, B.A., Bacon, J.R., 1991. Photophysics and photochemistry of oxygen sensors based on luminescent transition-metal complexes. Analytical Chemistry 63, 337–342.

Costerton, J.W., Lewandowski, Z., Caldwell, D.E., Korber, D.R., Lappin-Scott, H.M., 1995. Microbial biofilms. Annual Review of Microbiology 49, 711–745.

Costerton, J.W., Stewart, P.S., Greenberg, E.P., 1999. Bacterial biofilms: a common cause of persistent infections. Science 284, 1318–1322.

De Beer, D., Costerton, J.W., 2006. Microbial biofilms. In: Dworkin, M., Falkow, S., Rosenberg, E., Schleifer, K.H., Stackebrandt, E. (Eds.), Prokaryoteseds. Springer, New York, pp. 904–937.

De Beer, D., Stoodley, P., Roe, F., Lewandowski, Z., 1994. Effects of biofilm structures on oxygen distribution and mass transport. Biotechnology and Bioenginering 43, 1131–1138.

Eberl, H.J., Picioreanu, C., Heijnen, J.J., van Loosdrecht, M.C.M., 2000. A three-dimensional numerical study on the correlation of spatialstructure, hydrodynamic conditions, and mass transfer and conversionin biofilms. Chemical Engineering Science 55, 6209–6222.

Fenchel, T., Finlay, B., 2008. Oxygen and the spatial structure of microbial communities. Biological Reviews 83, 553–569.
Glud, R.N., Ramsing, N.B., Gundersen, J.K., Klimant, I., 1996. Planar optrodes: a new tool for fine scale measurements of two-dimensional O_2 distribution in benthic communities. Marine Ecology Progress Series 140, 217–226.
Glud, R.N., Santegoeds, C.M., de Beer, D., Kohls, O., Ramsing, N.B., 1998. Oxygen dynamics at the base of a biofilm studied with planar optrodes. Aquatic Microbial Ecology 14, 223–233.
Glud, R.N., Kühl, M., Kohls, O., Ramsing, N.B., 1999. Heterogenity of oxygen production and consumption in a photosynthetic microbial mat as studied by planar optodes. Journal of Phycology 35, 270–279.
Glud, R.N., 2008. Oxygen dynamics of marine sediments. Marine Biology Research 4, 243–289.
Hall-Stoodley, L., Costerton, J.W., Stoodley, P., 2004. Bacterial biofilms: from the natural environment to infectious diseases. Nature Reviews Microbiology 2, 95–108.
Hidalgo, G., Burns, A., Herz, E., Hay, A.G., Houston, P.L., Wiesner, U., Lion, L.W., 2009. Functional tomographic fluorescence imaging of pH microenvironments in microbial biofilms by use of silica nanoparticle sensors. Applied and Environmental Microbiology 75 (23), 7426–7435.
Holst, G., Grunwald, B., 2001. Luminescence lifetime imaging with transparent oxygen optodes. Sensors & Actuators, B: Chemical 74, 78–90.
Holst, G., Kohls, O., Klimant, I., Konig, B., Kühl, M., Richter, T., 1998. A modular luminescence lifetime imaging system for mapping oxygen distribution in biological samples. Sensors and Actuators B: Chemical 51, 163–170.
Huettel, M., Ziebis, W., Forster, S., 1996. Flow-induced uptake of particulate matter in permeable sediments. Limnology and Oceanography 41, 309–322.
Ivleva, N.P., Wagner, M., Horn, H., Niesner, R., Haisch, C., 2010. Raman microscopy and surface-enhanced Raman scattering (SERS) for in situ analsysis of biofilms. Journal of Biophotonics 3 (8–9), 548–556.
Jørgensen, B.B., Des Marais, D.J., 1990. The diffusive boundary layer of sediments: oxygen microgradients over a microbial mat. Limnology & Oceanography 35, 1343–1355.
Kühl, M., Rickelt, L.F., Thar, R., 2007. Combined imaging of bacteria and oxygen in biofilms. Applied and Environmental Microbiology 73 (19), 6289–6295.
Kühl, M., Glud, R.N., Ploug, H., Ramsing, N.B., 1996. Microenvironmental control of photosynthesis and photosynthesis-coupled respiration in an epilithic cyanobacterial biofilm. Journal of Phycology 32, 799–812.
Kühl, M., Jørgensen, B.B., 1992. Microsensor measurements of sulfate reduction and sulfide oxidation in compact microbial communities of aerobic biofilms. Applied and Environmental Microbiology 58, 1164–1174.
Kühl, M., 2005. Optical microsensors for analysis of microbial communities. Methods in Enzymology 397, 166–199.
Kühl, M., Polerecky, L., 2008. Functional and structural imaging of phototrophic microbial commmunities and symbioses. Aqautic Microbial Ecology 53, 99–118.
Larsen, M., Borisov S.M., Grunwald B., Klimant I. and Glud R.N. A simple and inexpensive high resolution color ratiometric planar optode imaging approach: application to oxygen and pH sensing. Limnology & Oceanography Methods, in press.
Neu, T.R., Manz, B., Volke, F., Dynes, J.J., Hitchcock, A.P., Lawrence, J.R., 2010. Advanced imaging techniques for assessment of structure, composition and function in biofilm systems. FEMS Microbiology Ecology 72, 1–21.
Nicolella, C., van Loosdrecht, M.C.M., Heijnen, S.J., 2000. Particle-based biofilm reactor technology. Trends in Biotechnology 18, 312–320.
Nielsen, L.P., Christensen, P.B., Revsbech, N.P., Sørensen, N.P., 1990. Denitrification and oxygen respiration in biofilms studied with a microsensor for nitrous oxide and oxygen. Microbial Ecology 19, 63–72.
Oguri, K., Kitazato, H., Glud, R.N., 2006. Platinum octaetylporphyrin based planar optodes combined with an UV-LED excitation light source: an ideal tool for high-resolution O_2 imaging in O_2 depleted environments. MarineChemistry 100, 95–107.
Polerecky, L., Franke, U., Werner, U., Grunwald, B., de Beer, D., 2005. High spatial resolution measurement of oxygen consumption rates in permeable sediments. Limnology and Oceanography: Methods 3, 75–85.
Revsbech, N.P., 2005. Analysis of microbial communities with electrochemical microsensors and microscale biosensors. Methods in Enzymology 397, 147–166.
Ridgway, H.F., Flemming, H.F., 1996. Membrane biofouling. In: Mallevialle, J., Odendaal, P.E., Wiesner, M.R. (Eds.), Water Treatment Membrane Processes. McGraw-Hill, New York, pp. 6.1–6.62.
Satoh, H., Sasaki, Y., Nakamura, Y., Okabe, S., Suzuki, T., 2005. Use of microelectrodes to investigate the effects of 2-chlorophenol on microbial activities in biofilms. Biotechnology and Bioengineering 91, 133–138.
Staal, M., Borisov, S.M., Rickelt, L.F., Klimant, I., Kühl, M., 2011. Ultrabright planar optodes for luminescence life-time based microscopic imaging of O_2 dynamics in biofilms. Journal of Microbial Methods 85, 67–74.
Stewart, P.S., Franklin, M.J., 2008. Physiological heterogeneity in biofilms. Nature Reviews Microbiology 6, 199–210.
Stoodley, P., deBeer, D., Lewandowski, Z., 1994. Liquid flow in biofilm systems. Applied and Environmental Microbiology 60, 2711–2716.
Vrouwenvelder, J.S., van Paassen, J.A.M., Wessels, L.P., van Dam, A.F., Bakker, S.M., 2006. The Membrane fouling simulator: a practical tool for fouling prediction and control. Journal of Membrane Science 281 (1–2), 316–324.
Vrouwenvelder, J.S., Bakker, S.M., Cauchard, M., Le Grand, R., Apacandie, M., Idrissi, M., Lagrave, S., Wessels, L.P., van Paassen, J.A.M., Kruithof, J.C., van Loosdrecht, M.C.M., 2007. The membrane fouling simulator: a suitable tool for prediction and characterisation of membrane fouling. Water Science & Technology 55 (8–9), 197–205.
Vrouwenvelder, J.S., Manolarakis, S.A., van der Hoek, J.P., van Paassen, J.A.M., van der Meer, W.G.J., van Agtmaal, J.M.C., Prummel, H.D.M., Kruithof, J.C., van Loosdrecht, M.C.M., 2008. Quantitative biofouling diagnosis in full scale nanofiltration and reverse osmosis installations. Water Research 42, 4856–4868.
Vrouwenvelder, J.S., Hinrichs, C., Van der Meer, W.G.J., Van Loosdrecht, M.C.M., Kruithof, J.C., 2009a. Pressure drop increase by biofilm accumulation in spiral wound RO and NF membrane systems: role of substrate concentration, flow velocity, substrate load and flow direction. Biofouling 25, 543–555.
Vrouwenvelder, J.S., Van Paassen, J.A.M., Kruithof, J.C., Van Loosdrecht, M.C.M., 2009b. Sensitive pressure drop measurements of individual lead membrane elements for accurate early biofouling detection. Journal of Membrane Science 338, 92–99.
Wagner, M., Manz, B., Volke, F., Neu, T.R., Horn, H., 2010. Online3 assessment of biofilm development, sloughing and forced detachment in tube reactor by means of magnetic resonance microscopy. Biotechnology and Bioengineering 107 (1), 172–181.
Wang, X., Meier, R.J., Link, M., Wolfbeis, O.S., 2010. Photographing oxygen distribution. Angewandte Chemie 122, 5027–5029.